Microphase Separation in Starblock Copolymer Melts

M. W. Matsen*,† and M. Schick

Department of Physics FM-15, University of Washington, Seattle, Washington 98195

Received May 25, 1994; Revised Manuscript Received August 11, 1994®

ABSTRACT: We examine the phase diagram of starblock copolymers with monodisperse diblock arms. Within a self-consistent-field theory, we calculate the phase diagrams for starblocks with equal Kuhn lengths for all monomers, and M = 1, 3, 5, and 9 arms. For M = 1 and 5, we also consider the effect of asymmetric Kuhn lengths. We find all phase diagrams to be topologically identical to that of diblocks (M = 1). In each case, the lamellar, gyroid, hexagonal, and cubic phases are found to be stable. The region of stability of the gyroid phase is found to increase as the number of arms is increased. Regions in which the double-diamond and catenoid-lamellar phases are nearly stable are also located.

1. Introduction

Melts of AB-type copolymer molecules have received much attention over the past few years due in a large part to their ability to assemble into various ordered structures. The mechanism that drives the system to form these structures is well understood. The A and B blocks of the copolymer tend to separate, forming A- and B-rich regions, in order to reduce the number of energetically unfavorable contacts between these blocks. In addition, the fact that the melt is essentially incompressible requires that the monomer density must remain uniform. The constraint imposed by the chemical junction of the A and B blocks implies that the A- and B-rich regions remain microscopic in size. Consequently a structure develops with an extensive amount of internal interface between the A- and B-rich regions. The microscopic scale of the structure is set by competing tendencies: one, decreasing the amount of unfavorable interface increases the scale, while the other, reducing the stretching of the polymer decreases it. The latter tendency arises from considerations which are primarily entropic; fewer configurations are accessible to polymers which are stretched.

The actual structure which forms at a given scale is determined by a competition between the two blocks, one composed of A and the other of B monomers, as to which of them will have to pay the entropic penalty of stretching. Both of the blocks would prefer to be on the convex side of a curved interface which would give them more available volume close to the interface, allowing them to relax. The competition is governed by the relative degrees of polymerization of the two blocks. If the two blocks have comparable monomer fractions, then the balanced competition would result in flat interfaces. If they are not comparable, it is entropically favorable for a curved interface to be formed in which the block with the larger monomer fraction relaxes on the convex side and the smaller block stretches on the concave side. As the asymmetry is made larger, it becomes favorable to form structures with larger mean curvature, which leads to the usual progression from a lamellar phase (L), to one with a hexagonal packing of cylinders (H), to a body-centered-cubic packing of spheres (C). An asymmetry in the Kuhn lengths also effects the competition, because the monomers with the longer Kuhn length can stretch a given amount with less of an entropic penalty. Thus it is favorable to have the blocks with the longer Kuhn length on the inside of curved surfaces.

The existence of lamellar, hexagonal, and cubic phases is well established in copolymer melts. Numerous other periodic structures which might be stable have been proposed.[1] Many of them are characterized by a constant mean curvature[2] whose value is intermediate between that of cylinders and of flat planes. Because the curvature of a structure depends inversely on the scale of that structure and the scale is determined by the competition between the energy of the internal interfaces and the stretching, both of which depend upon the structure itself, it is not possible *a priori* to state whether any of these phases are in fact stable. Some of them have been observed, although it does not necessarily follow that they are equilibrium phases. They are the double-diamond (OBDD)[3–8] gyroid (G),[9–11] monocontinuous catenoid-lamellar (MCL),[3,12,13] and bicontinuous catenoid-lamellar (BCL)[4] phases. The double-diamond and gyroid phases are similar to one another; in both phases the minority component forms two separate interweaving lattices with the majority component filling the space between. One difference between them is that the double-diamond phase has a 4-fold coordinated structure, while the gyroid phase has a 3-fold coordinated one. The catenoid-lamellar phases are ones in which the lamellae are perforated by a hexagonal arrangement of holes. In the monocontinuous version, only the minority-component lamellae are perforated, while in the bicontinuous one, all of the lamellae are. Experiments find the lamellae to be stacked with the holes staggered from layer to layer, but the sequence has not been determined. We examine both the *abab*... and *abcabc*... sequences. In refs 14 and 15 two separate hexagonally-structured lamellar phases were observed. They could be monocontinuous and bicontinuous catenoid-lamellar phases, and we will have more to say about this in section 3.

Fetters and co-workers first synthesized starblock copolymers with diblock arms nearly 20 years ago.[16] It has been shown[5,9] that the phase diagram for such melts is very similar to that of diblocks and that they can exhibit lamellar, double-diamond, gyroid, hexagonal, and cubic phases. Although there has been a considerable amount of experimental work[5–7,9,12,17,18] on these systems, there has been little theoretical work. Even the phase diagram for $(AB)_M$ starblocks has not been investigated extensively. References 19 and 20 have both calculated the spinodal line for several cases. In the latter reference, the critical point was located. Dobrynin and Erukhimovich[21] examined the phase diagram using a Landau–Ginzburg expansion with a truncated set of wavevectors. They did not

* To whom correspondence should be addressed.
† Present address: Department of Chemical Engineering and Materials Science, University of Minnesota, Minneapolis, MN 55455.
® Abstract published in *Advance ACS Abstracts,* October 1, 1994.

0024-9297/94/2227-6761$04.50/0

examine the double-diamond, catenoid-lamellar, and gyroid phases. Their approach assumes that the monomer densities in the ordered phases differ from those in the disordered phase by only a small amount and are therefore limited to very weak segregations. For strong segregations, Anderson and Thomas[2] investigated the stability of the double-diamond phase using a theory related to that of Ohta and Kawasaki[22] but did not find the phase to be stable.

In this paper, we consider melts of starblocks composed of identical AB diblock arms and explore the phase diagram as a function of the number of arms and the ratio of Kuhn lengths between outer and inner blocks. In all cases, we find the phase diagram to be topologically equivalent to that of the AB diblock system. That is we find the lamellar, gyroid, hexagonal, and cubic phases to have regions of stability. Further, the region of the gyroid phase can be enhanced either by increasing the number of arms or by altering the ratio of the Kuhn lengths. We also find other phases that are nearly stable between the lamellar and hexagonal phases. For weak segregations, the bicontinuous catenoid-lamellar phase is nearly stable, and for intermediate segregations, the monocontinuous catenoid-lamellar and the double-diamond phases are nearly stable also. We are unable to explore strongly segregated melts due to computational limitations.

2. Theory

We consider a system of n starblock copolymers each having M arms joined together at a central core. Each arm is an AB diblock where the A and B blocks consist of fN and $(1-f)N$ monomers, respectively. They are attached to the core by their A ends. We assume that the A and B monomers each occupy a fixed volume, $1/\rho_0$, and that the system is incompressible with a total volume, V, equal to nMN/ρ_0. The Kuhn lengths of A and B monomers are a_A and a_B, respectively. Each polymer is parametrized with a variable, s, that increases continuously along each arm. The core of the polymer corresponds to $s = 0$. Along the first arm, s increases from 0 at the inner end to f at the junction point and then to 1 at the outer end. Along each successive arm, s increases by 1, until $s = M$ at the end of the last arm. Using this parametrization, we define functions, $\mathbf{r}_\alpha(s)$, that specify configuration of the αth copolymer. We note that $\mathbf{r}_\alpha(s)$ is only a piecewise continuous function with discontinuities at integer values of s.

Having specified the system, we turn to a brief derivation of the self-consistent-field theory (SCFT) which describes it. In doing so, we follow Hong and Noolandi.[23] The partition function of the system is written as

$$Z = \int \left(\prod_{\alpha=1}^{n} \mathcal{D}\mathbf{r}_\alpha\, P[\mathbf{r}_\alpha;0,M]\right)\delta[1-\hat{\phi}_A-\hat{\phi}_B] \exp\left\{-\frac{\rho_0}{N}\int d\mathbf{r}\, \chi N\hat{\phi}_A(\mathbf{r})\,\hat{\phi}_B(\mathbf{r})\right\} \quad (1)$$

where the functional integral is over all configurations of the system. The δ functional selects out those configurations satisfying the incompressibility constraint. Configurations of individual polymers are weighted by the functional

$$P[\mathbf{r}_\alpha;s_1,s_2] \propto \exp\left\{-\frac{3}{2N}\int_{s_1}^{s_2} ds \left[\frac{\gamma(s)}{a_A^2}+\frac{1-\gamma(s)}{a_B^2}\right]\left|\frac{d}{ds}\mathbf{r}_\alpha(s)\right|^2\right\} \quad (2)$$

where $\gamma(s) = 1$ when s corresponds to an A-monomer region of the copolymer and is 0 for a B-monomer region. The dimensionless A- and B-monomer-density operators in eq 1 are given by

$$\hat{\phi}_A(\mathbf{r}) = \frac{N}{\rho_0}\sum_{\alpha=1}^{n}\int_0^M ds\, \gamma(s)\,\delta(\mathbf{r}-\mathbf{r}_\alpha(s)) \quad (3)$$

$$\hat{\phi}_B(\mathbf{r}) = \frac{N}{\rho_0}\sum_{\alpha=1}^{n}\int_0^M ds\, (1-\gamma(s))\delta(\mathbf{r}-\mathbf{r}_\alpha(s)) \quad (4)$$

The Flory–Huggins parameter, χ, measures the incompatibility between A and B monomers.[24] To make the expression for the partition function more tractable, one inserts functional integrals over δ functionals, $1 = \int \mathcal{D}\Phi_A\, \mathcal{D}\Phi_B\, \delta[\Phi_A-\hat{\phi}_A]\, \delta[\Phi_B-\hat{\phi}_B]$, which permits the replacement of the product of operators, $\hat{\phi}_A\hat{\phi}_B$, in eq 1 by the product of functions, $\Phi_A\Phi_B$, as well as the replacement of operators by functions in $\delta[1-\hat{\phi}_A-\hat{\phi}_B]$. One then inserts an integral representation in the δ functionals of the form

$$\delta[\Phi_A-\hat{\phi}_A] = \mathcal{N}\int \mathcal{D}W_A \exp\left\{\frac{\rho_0}{N}\int d\mathbf{r}\, W_A(\mathbf{r})\,[\Phi_A(\mathbf{r})-\hat{\phi}_A(\mathbf{r})]\right\} \quad (5)$$

$$\delta[1-\Phi_A-\Phi_B] = \mathcal{N}\int \mathcal{D}\Xi \exp\left\{\frac{\rho_0}{N}\int d\mathbf{r}\, \Xi(\mathbf{r})\,[1-\Phi_A(\mathbf{r})-\Phi_B(\mathbf{r})]\right\} \quad (6)$$

where $\mathcal{N}$ is a normalization constant and the limits of integration are $\pm i\infty$. These insertions bring the partition function into the form

$$Z = \mathcal{N}^3\int \mathcal{D}\Phi_A\, \mathcal{D}W_A\, \mathcal{D}\Phi_B\, \mathcal{D}W_B\, \mathcal{D}\Xi \exp\{-F[\Phi_A,W_A,\Phi_B,W_B,\Xi]/k_BT\} \quad (7)$$

with

$$F[\Phi_A,W_A,\Phi_B,W_B,\Xi]/nMk_BT \equiv -M^{-1}\ln \mathcal{Q}[W_A,W_B] + V^{-1}\int d\mathbf{r}\,[\chi N\Phi_A(\mathbf{r})\,\Phi_B(\mathbf{r}) - W_A(\mathbf{r})\,\Phi_A(\mathbf{r}) - W_B(\mathbf{r})\,\Phi_B(\mathbf{r}) - \Xi(\mathbf{r})\,(1-\Phi_A(\mathbf{r})-\Phi_B(\mathbf{r}))] \quad (8)$$

and

$$\mathcal{Q}[W_A,W_B] \equiv \int \mathcal{D}\mathbf{r}_\alpha\, P[\mathbf{r}_\alpha;0,M] \exp\{-\int_0^M ds\,[\gamma(s)\,W_A(\mathbf{r}_\alpha(s)) + (1-\gamma(s))W_B(\mathbf{r}_\alpha(s))]\} \quad (9)$$

This last quantity, $\mathcal{Q}[W_A,W_B]$, is simply the partition function of a single noninteracting polymer in external fields, $W_A(\mathbf{r})$ and $W_B(\mathbf{r})$. The above transformation is exact.

The functional $F[\Phi_A,W_A,\Phi_B,W_B,\Xi]$ can be evaluated exactly, but the functional integral in eq 7 cannot be carried out. In the SCFT,[23] the integral is evaluated using the saddle-point approximation, and thereby the free energy, $-k_BT\ln Z$, is approximated by $F[\phi_A,w_A,\phi_B,w_B,\xi]$, where ϕ_A, w_A, ϕ_B, w_B, and ξ are the functions for which F attains its minimum. From its definition, eq 8, it follows that these functions satisfy the self-consistent equations,

$$w_A(\mathbf{r}) = \chi N\phi_B(\mathbf{r}) + \xi(\mathbf{r}) \quad (10)$$

$$w_B(\mathbf{r}) = \chi N\phi_A(\mathbf{r}) + \xi(\mathbf{r}) \tag{11}$$

$$\phi_A(\mathbf{r}) + \phi_B(\mathbf{r}) = 1 \tag{12}$$

$$\phi_A = -\frac{V}{MQ}\frac{\mathcal{D}Q}{\mathcal{D}w_A} \tag{13}$$

$$\phi_B = -\frac{V}{MQ}\frac{\mathcal{D}Q}{\mathcal{D}w_B} \tag{14}$$

The last two equations identify $\phi_A(\mathbf{r})$ and $\phi_B(\mathbf{r})$ as the average densities of A and B monomers at $\mathbf{r}$ as calculated in the ensemble of the noninteracting polymers subject to external fields which are calculated self-consistently from eqs 10 and 11. Thus the saddle-point approximation has reduced the problem of interacting polymers to one of a single noninteracting polymer in external fields, $w_A(\mathbf{r})$ and $w_B(\mathbf{r})$. Once the partition function of the latter problem, $Q[w_A,w_B]$, is known, the set of equations 10–14 can be solved.

To calculate the partition function, Q, one first writes it in terms of the end-segment distribution function $q(\mathbf{r},s)$,

$$Q = \int d\mathbf{r}\, q(\mathbf{r},1) \tag{15}$$

where

$$q(\mathbf{r},s) = \int d\mathbf{r}'\, [q^\dagger(\mathbf{r}',1)]^{M-1} \int \mathcal{D}\mathbf{r}_\alpha\, P[\mathbf{r}_\alpha;0,s]\, \delta(\mathbf{r}'-\mathbf{r}_\alpha(0))\, \delta(\mathbf{r}-\mathbf{r}_\alpha(s))\, \exp\{-\int_0^s dt\, [\gamma(t)\, w_A(\mathbf{r}_\alpha(t)) + (1-\gamma(t))w_B(\mathbf{r}_\alpha(t))]\} \tag{16}$$

which is defined in terms of a second distribution function,

$$q^\dagger(\mathbf{r},s) = \int \mathcal{D}\mathbf{r}_\alpha\, P[\mathbf{r}_\alpha;s,1]\, \delta(\mathbf{r}-\mathbf{r}_\alpha(s))\, \exp\{-\int_s^1 dt\, [\gamma(t)\, w_A(\mathbf{r}_\alpha(t)) + (1-\gamma(t))w_B(\mathbf{r}_A(t))]\} \tag{17}$$

These two end-segment distribution functions are only defined on the interval $0 \le s \le 1$. They are evaluated by solving the modified diffusion equations[25]

$$\frac{\partial}{\partial s} q(\mathbf{r},s) = \begin{cases} \frac{1}{6}Na_A^2\nabla^2 q(\mathbf{r},s) - w_A(\mathbf{r})\, q(\mathbf{r},s), & \text{if } 0 < s < f \\ \frac{1}{6}Na_B^2\nabla^2 q(\mathbf{r},s) - w_B(\mathbf{r})\, q(\mathbf{r},s), & \text{if } f < s < 1 \end{cases} \tag{18}$$

$$\frac{\partial}{\partial s} q^\dagger(\mathbf{r},s) = \begin{cases} -\frac{1}{6}Na_A^2\nabla^2 q^\dagger(\mathbf{r},s) + w_A(\mathbf{r})\, q^\dagger(\mathbf{r},s), & \text{if } 0 < s < f \\ -\frac{1}{6}Na_B^2\nabla^2 q^\dagger(\mathbf{r},s) + w_B(\mathbf{r})\, q^\dagger(\mathbf{r},s), & \text{if } f < s < 1 \end{cases} \tag{19}$$

under the conditions $q(\mathbf{r},0) = [q^\dagger(\mathbf{r},0)]^{M-1}$ and $q^\dagger(\mathbf{r},1) = 1$ for all $\mathbf{r}$. Note that one must solve for $q^\dagger(\mathbf{r},s)$ prior to solving for $q(\mathbf{r},s)$. In terms of these end-segment distribution functions, the A-monomer density, eq 13, can be written as

$$\phi_A(\mathbf{r}) = \frac{V}{Q}\int_0^f ds\, q(\mathbf{r},s)\, q^\dagger(\mathbf{r},s) \tag{20}$$

where the fact that each arm of the polymers contributes equally to the density has been used. The expression for $\phi_B(\mathbf{r})$ is similar.

Once a solution of the self-consistent equations is found, the free energy of that solution is $F[\phi_A,w_A,\phi_B,w_B,\xi]$ of eq 8. Rather than attempting to solve the above self-consistent equations in real space, we expand all functions of position in a convenient set of orthonormal basis functions $f_i(\mathbf{r})$, $i = 1, 2, 3, \ldots$:

$$g(\mathbf{r}) = \sum_i g_i f_i(\mathbf{r}) \tag{21}$$

with

$$\frac{1}{V_{cell}}\int_{cell} f_i(\mathbf{r})\, f_j(\mathbf{r})\, d\mathbf{r} = \delta_{ij} \tag{22}$$

We take the basis functions to be eigenfunctions of the Laplacian operator:

$$\nabla^2 f_i(\mathbf{r}) = -\frac{\lambda_i}{D^2} f_i(\mathbf{r}) \tag{23}$$

The length scale, D, and the choice of V_{cell} are discussed below. We order the functions such that λ_i is a nondecreasing series. The first basis function is then $f_1(\mathbf{r}) = 1$ with an eigenvalue $\lambda_1 = 0$.

In this basis, the diffusion equations, 18 and 19, become

$$\frac{dq_i(s)}{ds} = \begin{cases} \sum_j A_{ij} q_j(s), & \text{if } 0 < s < f \\ \sum_j B_{ij} q_j(s), & \text{if } f < s < 1 \end{cases} \tag{24}$$

$$\frac{dq_i^\dagger(s)}{ds} = \begin{cases} -\sum_j A_{ij} q_j^\dagger(s), & \text{if } 0 < s < f \\ -\sum_j B_{ij} q_j^\dagger(s), & \text{if } f < s < 1 \end{cases} \tag{25}$$

where the matrix, A, is given by

$$A_{ij} = -\frac{Na_A^2\lambda_i}{6D^2}\delta_{ij} - \sum_k w_{A,k}\Gamma_{ijk} \tag{26}$$

with

$$\Gamma_{ijk} = \frac{1}{V_{cell}}\int_{cell} f_i(\mathbf{r})\, f_j(\mathbf{r})\, f_k(\mathbf{r})\, d\mathbf{r} \tag{27}$$

The matrix, B, is given by a similar expression. First $q_i^\dagger(s)$ is solved starting with $q_i^\dagger(1) = 1$, and then $q_i(s)$ is solved using $q_i(0) = \psi_i^{M-1}$ where

$$\psi_i^{(m)} \equiv \frac{1}{V_{cell}}\int_{cell} d\mathbf{r}\, [q^\dagger(\mathbf{r},0)]^m f_i(\mathbf{r}) \tag{28}$$

These amplitudes are determined using $\psi_i^{(1)} = q_i^\dagger(0)$ together with the relation $\psi_i^{(m+n)} = \sum_{jk}\psi_j^{(m)}\psi_k^{(n)}\Gamma_{ijk}$.

These sets of linear differential equations can easily be solved by performing an orthogonal transformation to diagonalize A if $s < f$ or B if $s > f$. The resulting solutions are

$$q_i(s) = \begin{cases} \sum_j T_{A,ij}(s)\, \psi_j^{M-1}, & \text{if } 0 < s < f \\ \sum_{jk} T_{B,ij}(s-f) T_{A,jk}(f) \psi_k^{M-1}, & \text{if } f < s < 1 \end{cases} \tag{29}$$

$$q_i^{\dagger}(s) = \begin{cases} \sum_j T_{A,ij}(f-s)T_{B,j1}(1-f), & \text{if } 0 < s < f \\ T_{B,i1}(1-s), & \text{if } f < s < 1 \end{cases} \quad (30)$$

where $T_A(s')$ and $T_B(s')$ are matrices that transfer $q_i(s)$ a distance s' along A and B regions of the first arm, respectively. Similarly, they transfer $q_i^{\dagger}(s)$ a distance $-s'$.

Now that the amplitudes of the end-segment distribution functions are known, Q is given by $Vq_1(1)$, and the amplitudes of $\phi_A(\mathbf{r})$, eq 20, are

$$\phi_{A,i} = \frac{1}{q_1(1)}\int_0^f ds \sum_{jk} q_j(s)\, q_k^{\dagger}(s)\, \Gamma_{ijk} \quad (31)$$

The amplitudes of $\phi_B(\mathbf{r})$ are given by a similar expression. We must now adjust the assumed amplitudes $w_{A,i}$ and $w_{B,i}$ of the fields so that the densities calculated from them above satisfy the incompressibility condition, eq 12,

$$\phi_{A,i} + \phi_{B,i} = 0, \quad i = 2, 3, \ldots \quad (32)$$

and, in addition, are related to the monomer-density amplitudes via eqs 10 and 11:

$$w_{A,i} - w_{B,i} + \chi N(\phi_{A,i} - \phi_{B,i}) = 0, \quad i = 2, 3, \ldots \quad (33)$$

Without loss of generality, we can set the average value of $\xi(\mathbf{r})$, which is ξ_1, to zero so that $w_{A,1} = \chi N\phi_{B,1}$ and $w_{B,1} = \chi N\phi_{A,1}$. This completes the cycle of self-consistent equations.

Now the free energy of eq 8 can be written

$$\frac{F}{nMk_BT} = -\frac{1}{M}\ln(q_1(1)) - \chi N\sum_i \phi_{A,i}\phi_{B,i} \quad (34)$$

For the disordered phase, this expression reduces to $F/nMk_bT = \chi Nf(1-f)$. For a periodic, ordered phase of a certain symmetry, only eigenfunctions of the Laplacian with that symmetry[26] are included in the sequence of functions, $f_i(\mathbf{r})$. They are normalized within a unit cell of the phase, V_{cell}. The free energy still has to be minimized with respect to the wavelength, D, of the phase. For catenoid-lamellar phases, there are two such wavelengths: one of the lamellae and the other of the triangular arrangement of holes within each sheet. By comparing the free energies of different phases, we determine the phase diagram.

As a matter of practicality, only a limited number of basis functions are included in the expansion of spatially-dependent quantities. We have used a sufficient number of basis functions to achieve an accuracy of a part in 10^4 in the free energy. The number of functions needed to achieve this depends on the phase examined and the value of χN. We have employed up to 60 of them to obtain this accuracy.

3. Results and Discussion

Figures 1–4 show the phase diagrams for melts of starblock copolymers with 1, 3, 5, and 9 arms, respectively, for A and B monomers with identical Kuhn lengths. The one-arm starblock is just the diblock. Except for the critical points marked by a dot, all transitions are first order. The phase boundaries for the gyroid phase could not be calculated for strong segregations because the number of basis functions required to reproduce the sharp interfaces causes the calculation to exceed our computational facilities. We have therefore extrapolated the phase boundaries with dashed lines. Our extrapolation is done so that the gyroid phase maintains a uniform width over the metastable lamellar–hexagonal transition. From these figures, it can be concluded that there is a preference for the inner block of the arms to be located on the inside of cylindrical and spherical structures, a preference which increases with the number of arms. To see this, it should be recalled that the inner block, whose volume fraction is measured by f, is found in the interior of these structures

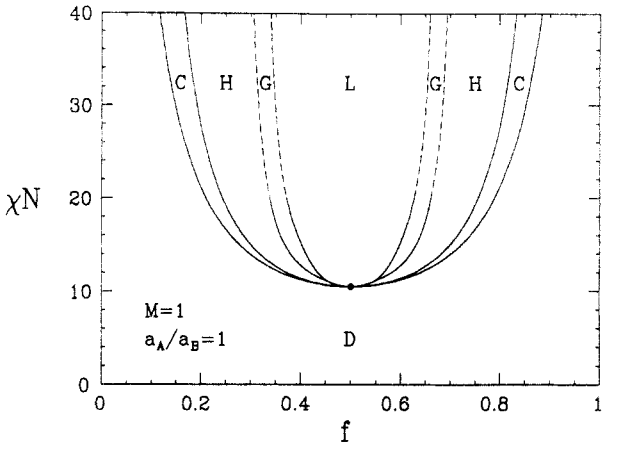

Figure 1. Phase diagram for a melt of diblocks with A and B monomers that have equal Kuhn lengths. The regions of stability for the disordered, lamellar, gyroid, hexagonal, and cubic phases are denoted D, L, G, H, and C, respectively. All transitions are first order except for the critical point which is marked by a dot. Dashed lines are extrapolated phase boundaries.

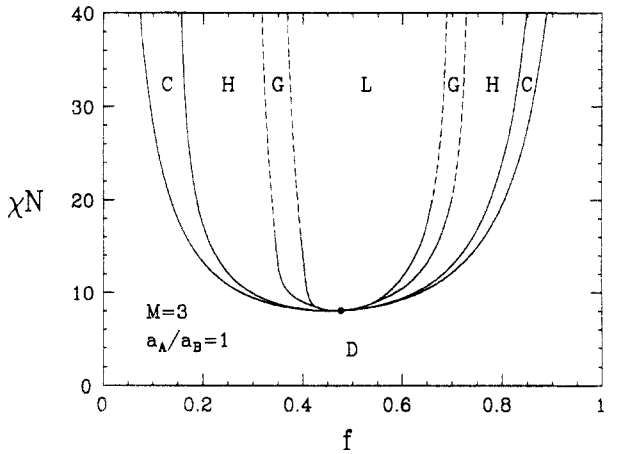

Figure 2. Phase diagram similar to Figure 1 but for a three-arm starblock melt.

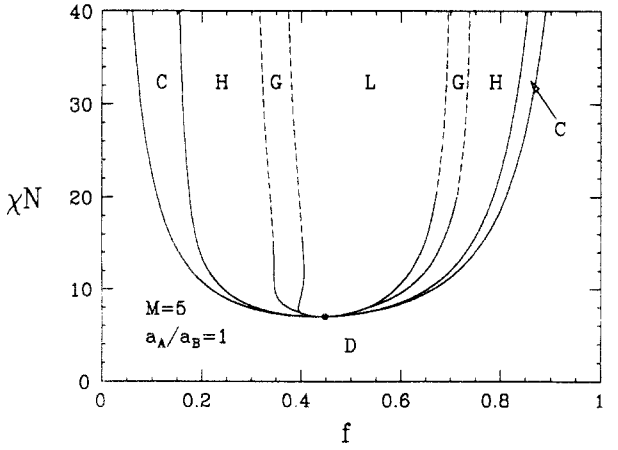

Figure 3. Phase diagram similar to Figure 1 but for a five-arm starblock melt.

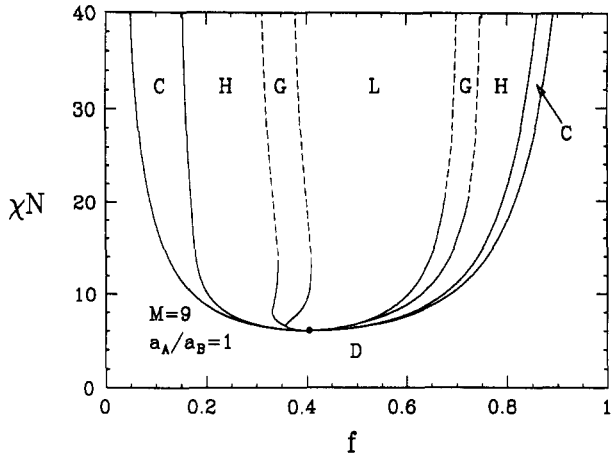

Figure 4. Phase diagram similar to Figure 1 but for a nine-arm starblock melt.

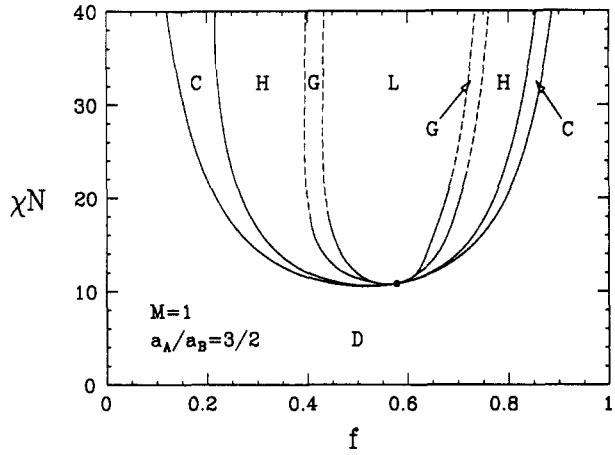

Figure 5. Phase diagram for a diblock melt when the ratio of Kuhn lengths of A and B monomers is 3:2.

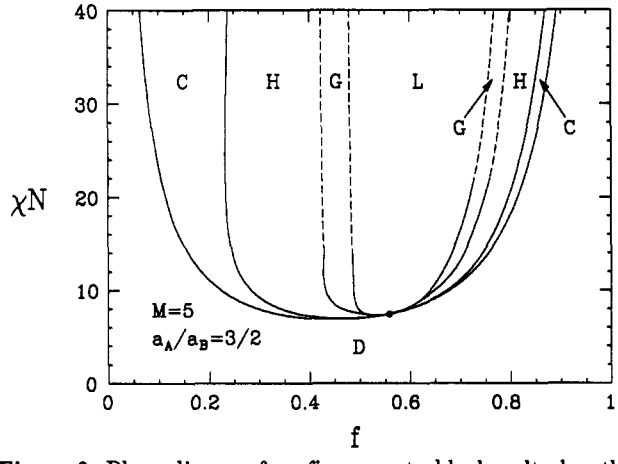

Figure 6. Phase diagram for a five-arm starblock melt when the ratio of Kuhn lengths for the monomers comprising the inner and outer blocks is 3:2.

when $f < 1/2$. As the regions of f over which the cylindrical (H) and cubic (C) phases are found increase with the number of arms when $f < 1/2$ and decrease when $f > 1/2$, the preference follows.

Figures 5–7 show phase diagrams for diblocks and five-arm starblocks with asymmetric Kuhn lengths. This asymmetry significantly alters the positions of the phase boundaries, but it does not change the topology of the phase diagram. Vavasour and Whitmore[27] had suggested that such an asymmetry might do so, but a recent calculation shows this not to be the case,[28] as do the results here. A comparison of Figures 3 and 6 shows that the

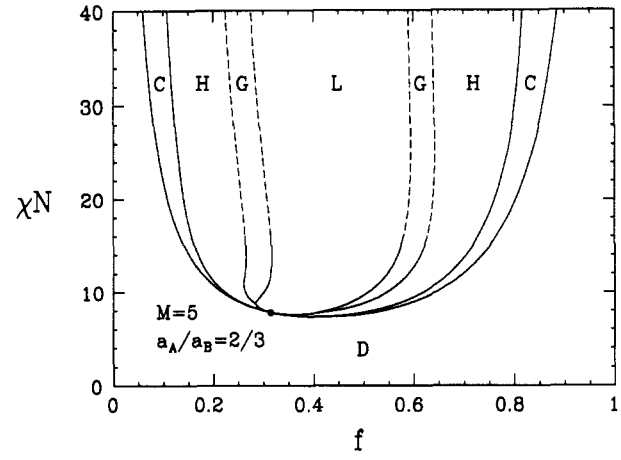

Figure 7. Phase diagram for a five-arm starblock melt when the ratio of Kuhn lengths for the monomers comprising the inner and outer blocks is 2:3.

Table 1. Location of the L + H + G Triple Points in the Phase Diagrams Shown in Figures 1–7[a]

M	a_A/a_B	χN	f	$D_L/aN^{1/2}$	$D_H/aN^{1/2}$	$D_G/aN^{1/2}$
1	1	11.14	0.452	1.34	1.55	3.31
3	1	8.49	0.424	1.39	1.59	3.41
3	1	8.96	0.544	1.42	1.64	3.50
5	1	7.45	0.398	1.35	1.54	3.30
5	1	7.96	0.533	1.40	1.63	3.48
9	1	6.55	0.358	1.28	1.46	3.12
9	1	6.93	0.512	1.36	1.59	3.38
1	3/2	11.04	0.528	1.35	1.56	3.33
1	3/2	11.82	0.617	1.35	1.56	3.32
5	3/2	7.44	0.511	1.45	1.65	3.53
5	3/2	8.95	0.622	1.48	1.72	3.66
5	2/3	7.76	0.406	1.33	1.55	3.30
5	2/3	8.70	0.285	1.27	1.46	3.11

[a] At each triple point, the lamellar spacing D_L, the spacing between cylinders D_H, and the size of the cubic unit cell D_G are given for the L, H, and G phases, respectively.

preference for the inner block to be located on the inside of cylindrical and spherical structures is enhanced it if has a larger Kuhn length than the outer block, a result in accord with the discussion in the Introduction. However, this preference can be reduced and even overcome if the outer block has the longer Kuhn length, as can be seen by comparing Figure 3 with Figure 7.

The most interesting aspect of these phase diagrams is the presence of a stable gyroid phase between the lamellar and hexagonal ones. Its location in the phase diagram is consistent with experiment. Hajduk et al.[10] studied a PS/PI diblock ($a_A/a_B = 0.85$[14]) of PS volume fraction $f = 0.33$ and observed this gyroid phase for χN between about 16 and 21. For these conditions we predict it to be stable for χN between 18 and 24. More recent experiments have found a stable G phase between the L and H phases for both six-arm and eighteen-arm starblock melts.[9] Unlike the lamellar, hexagonal, and cubic phases which all extend to a mean-field critical point, the gyroid phase terminates at a triple point. Consequently there is an interval of volume fractions within which the gyroid phase should not be observed. Table 1 gives the coordinates of all the triple points in Figures 1–7. Also given are the characteristic lengths of the three coexisting phases at each triple point. Even though the lengths D_L, D_H, and D_G vary significantly for the different triple points, the ratios D_G/D_L and D_G/D_H deviate little from the values 2.46 and 2.14, respectively. These ratios also show little change as one moves up the G–L and G–H phase boundaries. They are in good agreement with experimental results. Hajduk et al.[10] measured D_G/D_L to be 500 Å/210 Å ≈ 2.4, and Schulz

Table 2. Relative Scattering Intensities for the Gyroid Phase[a]

peak	meas				
(211)	yes	1.000 00	1.000 00	1.000 00	1.000 00
(220)	yes	0.109 57	0.123 03	0.110 89	0.120 20
(321)	no	0.000 18	0.001 62	0.002 14	0.000 59
(400)	no	0.000 10	0.000 37	0.000 44	0.000 02
(420)	yes	0.004 52	0.000 08	0.000 17	0.002 60
(332)	yes	0.002 06	0.000 11	0.000 80	0.001 58
(422)	no	0.001 38	0.000 04	0.000 01	0.001 17
(431)	no	0.001 01	0.000 08	0.000 00	0.001 07
(521)	no	0.002 48	0.000 64	0.001 45	0.001 10
(440)	yes	0.001 37	0.000 43	0.001 09	0.000 65
(532)	yes	0.002 46	0.000 92	0.002 20	0.001 38
(611)	yes	0.005 24	0.002 10	0.004 99	0.002 80

[a] Column two indicates the peaks observed in ref 10 for a PS/PI diblock melt, and column three shows our corresponding intensities with $f = 0.33$, $\chi N = 20$, and $a_A/a_B = 0.85$. The remaining three columns are for copolymer melts along the metastable L–H transitions at $\chi N = 15$ with $a_A = a_B$. The fourth column is for a diblock melt ($f = 0.3917$), and the fifth and sixth columns are for five-arm starblock melts ($f = 0.3858$ and 0.6568, respectively).

et al.[29] found that epitaxial growth from the H to the G phase would only occur if D_G/D_H were approximately $3/\sqrt{2} = 2.12$.

Because the experimental evidence for the gyroid phase is largely supported by small-angle X-ray scattering (SAXS) results, we have calculated scattering intensities for the gyroid phase in diblock and starblock melts at several locations where we find it to be stable. The scattering intensities of a given peak are simply proportional to the square of $\phi_{A,i}$, the density amplitude which is given in eq 31. In Table 2 we give the ratio of the intensity of a given peak normalized to that of the first nonzero peak, $(\phi_{A,i}/\phi_{A,2})^2$ for $i = 2$–13. Rather than index them by i, we employ the standard spectroscopic (lhk) notation used for cubic phases. The first coefficient $\phi_{A,1} = f$, which corresponds to (000), is omitted as it does not contribute to the scattering. The set of scattering intensities in column three pertains to a diblock with $a_A/a_B = 0.85$ appropriate for the PS/PI diblock,[14] at $\chi N = 20$ and $f = 0.33$, which are, approximately, the conditions under which ref 10 measured the SAXS intensity of this phase. To compare their experimental amplitudes with ours more precisely, we would have to apply a Lorentz correction to our results which would reduce the intensities monotonically with increasing wavenumbers, $(l^2 + k^2 + h^2)^{1/2}$, to a degree determined by experimental conditions. Rather than present such nonuniversal results, we leave our calculations uncorrected and simply indicate in column two whether a peak was observed or not in ref 10. Our results for the (321) and (400) intensities are calculated to be exceptionally small, which we believe explains the fact that they were not observed experimentally. We note that the amplitudes (532) and (611) correspond to wavevectors with the same magnitude and therefore would result in a single scattering peak (in a sample with randomly oriented domains). Their combined intensity is quite strong, and thus it is understandable that this peak was seen. The only surprising experimental result is that the small (440) peak was observed. In contrast to this result at $\chi N = 20$, we quote results for three cases at $\chi N = 15$ on the metastable L–H transition with symmetric Kuhn lengths. Column four is again for a diblock, while columns five and six are for the five-arm starblock. Other than the obvious trend that higher order reflections become weaker as the segregation is reduced, we find no general behavior in the scattering intensities. In particular, the near absence of the (321) and (400) intensities in ref 10 seems to be accidental. This result is consistent with the fact that ref 11 did observe the (400) peak using small-angle neutron scattering on an oriented sample. The orientation of their sample prevented them from observing a (321) peak.

Table 3. Free Energy Excess with Respect to the Stable Phase, ΔF, and Characteristic Length, D, for Various Phases of a Five-Arm Starblock at $\chi N = 15$ along the Two Metastable L–H Transitions with $a_A = a_B$[a]

phase	$\Delta F/nMk_BT$	$D/aN^{1/2}$	C/D	$\Delta F/nMk_BT$	$D/aN^{1/2}$	C/D
G	0.0	3.82		0.0	3.78	
MCL_{ab}	0.0036	1.55	1.32	0.0023	1.53	1.32
MCL_{abc}	0.0037	1.55	1.32	0.0023	1.53	1.33
L	0.0080	1.57		0.0038	1.54	
H	0.0080	1.77		0.0038	1.76	
BCL_{abc}	0.0263	1.57	1.23	0.0135	1.53	1.23
BCL_{ab}	0.0309	1.68	1.13	0.0169	1.60	1.16
C	0.0546	2.18		0.0237	2.16	
OBDD	0.0810	2.20		0.0423	2.05	
D	0.3334			0.1271		

[a] The entries on the left and right correspond to the cases where the inner block is the minority component ($f = 0.3858$) and the majority component ($f = 0.6568$), respectively. For the L and CL phases, D is the lamellar spacing, and for the H phase, it is the spacing between cylinders. For the C, G, and OBDD phases it is the size of their cubic unit cells. The ratio of the in-plane, C, to out-of-plane, D, lattice parameters is given for CL phases.

One aspect of all the copolymer phase diagrams examined which we find remarkable is the stability of the gyroid phase with respect to other nearly-stable phases, a stability which persists in spite of rather large changes of architecture. Table 3 shows just how close the free energies of the various phases are at a particular point in the phase diagram of the five-arm starblock. We expected that modest changes in the architecture would stabilize one of these other phases and make the gyroid metastable. However, we have not observed this to be the case when we have changed the number of arms, or the ratio of Kuhn lengths, as in this paper or replaced the diblock by a linear multiblock.[30] All of the architectures we have examined have in common that all A blocks have equal polymerization as do all the B blocks. Work by Shi and Noolandi[31] suggests that, if this condition is relaxed, the phase diagram can be significantly altered.

Because of nonequilibrium conditions attained in most experiments, it is of interest to consider phases which are nearly stable. In a previous work,[32] we discussed these phases and the locations where we found them to be nearly stable for diblock melts. In all cases, the regions of near stability were between the lamellar and hexagonal phases. Here we extend that discussion to include starblocks. For five-arm starblocks with symmetric Kuhn lengths ($a_A/a_B = 1$), Table 3 shows the relative stability of phases along the two metastable L–H transitions at $\chi N = 15$. The two monocontinuous catenoid-lamellar phases are very nearly stable in the same region over which the gyroid phase is stable. Although the MCL_{ab} and MCL_{abc} phases have nearly equal free energies, the former is slightly favored over the latter. For diblocks, the double-diamond phase is also nearly stable in this region, but for the starblocks ($M \neq 1$) this is no longer true. This is consistent with new observations for starblock melts which find some phases earlier identified as double-diamond to be, in reality, gyroid.[9] The bicontinuous catenoid-lamellar BCL_{abc} phase also becomes nearly stable, particularly for very weak segregations along the L–H transitions.

The most comprehensive experimental study of $(AB)_M$ starblocks is by Herman et al.[5] They examined 18-arm PI/PS starblocks over a wide range of volume fractions. In most cases the inner blocks were PI ($a_A/a_B = 1.17$), but in a few cases they were PS ($a_A/a_B = 0.85$). They observed

the sequence of phases C → H → L → OBDD → H → C as the volume fraction of the inner block increased from $f = 0.09$ to 0.91. (The phase identified as OBDD is now thought to be G.[9]) They did not observe the OBDD phase, or any other complex phase, between the L and H phase when the inner block formed the minority component. However, there is a reasonably large interval, $f = 0.37$–0.48, which they did not explore, so it is possible that such a phase does exist between the H and L phases in this region also.

The G phase (originally identified as OBDD) which occurs when the inner blocks form the majority component has been examined extensively. In addition to ref 5, refs 6 and 7 have examined its transition to the hexagonal phase in PI/PS starblocks in which PI is the inner block. In all cases, the volume fraction of that block was held constant at $f = 0.73$. An increase in the number of arms caused a transition from the hexagonal phase to the gyroid phase. This agrees with our result that the phase boundaries move to larger f as M increases (see Figures 1–4). In ref 6 it was observed that increasing N alone caused a transition from the H to the G phase, which is consistent with our phase diagrams when the inner blocks are the majority component.

There is experimental evidence for other unconventional phases. Although not observed in pure starblock copolymer melts, a monocontinuous catenoid-lamellar phase was observed by Hashimoto et al.[12] in a blend of starblocks and homopolymers. They also observed another phase composed of connected cylindrical units, much as in the OBDD and G phases. They concluded that it was not the ODBB phase. The G phase was not recognized as a possible equilibrium morphology at the time, and so they did not consider it.

Hashimoto et al.[17] have examined the weak-segregation region for a six-arm PI/PS starblock with an inner-arm volume fraction of $f = 0.73$. In order to work in the weak-segregation region, some solvent was added to the melt. By varying the temperature, they brought about the order-disorder transition. They identified the ordered phase as the hexagonal phase using SAXS data but admitted the presence of at least one unexplained peak. Identification of it as an OBDD phase would not account for this peak. It would be interesting to reexamine this region of the phase diagram and consider whether the phases were gyroid or catenoid-lamellar. It would also be of interest to explore the weak-segregation limit by examining lower weight starblocks as opposed to introducing a solvent.

In this work, fluctuations have not been considered. It is well established that their inclusion causes the critical point to vanish and direct first-order transitions between ordered phases and the disordered phase to appear.[33] These changes are consistent with experiment.[34] It has also been suggested that, at weak segregations, their inclusion stabilizes phases which are unstable within mean-field theory. In addition to this, they could affect the topology of a phase. For example, connecting catenoids might be broken or smeared out, causing a catenoid-lamellar phase to become simply a modulated-lamellar. This scenario suggests a possible relationship between our calculated catenoid-lamellar phases and the two hexagonally-structured lamellar phases observed in refs 14 and 15. Such hypotheses are worth further investigation.

Acknowledgment. We acknowledge useful conversations with A.-C. Shi, F. S. Bates, M. F. Schulz, E. L. Thomas, and D. A. Hajduk. We thank the Department of Physics at Simon Fraser University for use of their computing facilities and J. Shore for his help in this regard. This work was supported in part by the NSF, under Grant No. DMR 9220733, and NSERC of Canada.

References and Notes

(1) Scriven, L. E. *Nature* **1976**, *263*, 123.
(2) Anderson, D. M.; Thomas, E. L. *Macromolecules* **1988**, *21*, 3221.
(3) Spontak, R. J.; Smith, S. D.; Ashraf, A. *Macromolecules* **1993**, *26*, 956.
(4) Thomas, E. L.; Anderson, D. M.; Henkee, C. S.; Hoffman, D. *Nature* **1988**, *334*, 598.
(5) Herman, D. S.; Kinning, D. J.; Thomas, E. L.; Fetters, L. J. *Macromolecules* **1987**, *20*, 2940.
(6) Alward, D. B.; Kinning, D. J.; Thomas, E. L.; Fetters, L. J. *Macromolecules* **1986**, *19*, 215.
(7) Thomas, E. L.; Alward, D. B.; Kinning, D. J.; Martin, D. C.; Handlin, D. L., Jr.; Fetters, L. J. *Macromolecules* **1986**, *19*, 2197. Kinning, D. J.; Thomas, E. L.; Alward, D. B.; Fetters, L. J.; Handlin, D. L., Jr. *Macromolecules* **1986**, *19*, 1288.
(8) Hasegawa, H.; Tanaka, H.; Yamasaki, K.; Hashimoto, T. *Macromolecules* **1987**, *20*, 1651. Hashimoto, T.; Yamasaki, K.; Koizumi, S.; Hasegawa, H. *Macromolecules* **1993**, *26*, 2895.
(9) Some phases in starblock melts originally thought to be double-diamond have now been identified as gyroid. Hajduk, D. A.; Harper, P. E.; Gruner, S. M.; Honeker, C. C.; Thomas, E. L.; Fetters, L. J. *Macromolecules*, submitted.
(10) Hajduk, D. A.; Harper, P. E.; Gruner, S. M.; Honeker, C. C.; Kim, G.; Thomas, E. L.; Fetters, L. J. *Macromolecules* **1994**, *27*, 4063.
(11) Schulz, M. F.; Bates, F. S.; Almdal, K.; Mortensen, K. *Phys. Rev. Lett.* **1994**, *73*, 86.
(12) Hashimoto, T.; Koizumi, S.; Hasegawa, H.; Izumitani, T.; Hyde, S. T. *Macromolecules* **1992**, *25*, 1433.
(13) Disko, M. M.; Liang, K. S.; Behal, S. K.; Roe, R. J.; Jeon, K. J. *Macromolecules* **1993**, *26*, 2983.
(14) Almdal, K.; Koppi, K. A.; Bates, F. S.; Mortensen, K. *Macromolecules* **1992**, *26*, 1743.
(15) Hamley, I. W.; Koppi, K. A.; Rosedale, J. H.; Bates, F. S.; Almdal, K.; Mortensen, K. *Macromolecules* **1993**, *26*, 5959.
(16) Bi, L. K.; Fetters, L. J. *Macromolecules* **1976**, *9*, 732.
(17) Hashimoto, T.; Ijichi, Y.; Fetters, L. J. *J. Chem. Phys.* **1988**, *89*, 2463.
(18) Price, C.; Watson, A. G.; Chow, M. T. *Polymer* **1972**, *13*, 333.
(19) Benoit, H.; Hadziioannou, G. *Macromolecules* **1988**, *21*, 1449.
(20) Mayes, A. M.; Olvera de la Cruz, M. *J. Chem. Phys.* **1989**, *91*, 7228.
(21) Dobrynin, A. V.; Erukhimovich, I. Ya. *Macromolecules* **1988**, *21*, 1449.
(22) Ohta, T.; Kawasaki, K. *Macromolecules* **1980**, *13*, 1602.
(23) Hong, K. M.; Noolandi, J. *Macromolecules* **1981**, *14*, 727.
(24) Bates, F. S.; Schulz, M. F.; Rosedale, J. H.; Almdal, K. *Macromolecules* **1992**, *25*, 5547.
(25) Helfand, E. *J. Chem. Phys.* **1975**, *62*, 999.
(26) The unnormalized basis functions can be found in: *International Tables for X-Ray Crystallography*; Henry, N. F. M., Lonsdale, K., Eds.; Kynoch: Birmingham, U.K., 1969. Those of the OBDD and G phases appear on pp 515 and 524–5, respectively.
(27) Vavasour, J. D.; Whitmore, M. D. *Macromolecules* **1993**, *26*, 7070.
(28) Matsen, M. W.; Schick, M. *Macromolecules* **1994**, *27*, 4014.
(29) The authors of ref 11, through a careful reanalysis, have now concluded that the epitaxy which occurred in their experiment is the same one observed by: Clerc, M.; Levelt, A. M.; Sadoc, J. F. *J. Phys. II (Fr.)* **1991**, *1*, 2646.
(30) Matsen, M. W.; Schick, M. *Macromolecules*, submitted.
(31) Shi, A.-C.; Noolandi, J. *Macromolecules*, submitted.
(32) Matsen, M. W.; Schick, M. *Phys. Rev. Lett.* **1994**, *72*, 2660.
(33) Brazovskii, S. A. *Sov. Phys. JETP* **1975**, *41*, 85. Fredrickson, G. H.; Helfand, E. *J. Chem. Phys.* **1987**, *87*, 697. Mayes, A. M.; Olvera de la Cruz, M. *J. Chem. Phys.* **1991**, *95*, 4670. Muthukumar, M. *Macromolecules* **1993**, *26*, 5259.
(34) Bates, F. S.; Rosedale, J. H.; Fredrickson, G. H.; Glinka, C. J. *Phys. Rev. Lett.* **1988**, *61*, 2229. Almdal, K.; Bates, F. S.; Mortensen, K. *J. Chem. Phys.* **1992**, *96*, 9122.